

Parton saturation approach in heavy quark production at high energies

V.P. Gonçalves

*Instituto de Física e Matemática, Universidade Federal de Pelotas
Caixa Postal 354, CEP 96010-090, Pelotas, RS, Brazil
barros@ufpel.edu.br*

M.V.T. Machado^{a,b}

^a *Universidade Estadual do Rio Grande do Sul - UERGS
Unidade Bento Gonçalves, CEP 95700-000, Bento Gonçalves, RS, Brazil*
^b *High Energy Physics Phenomenology Group, GFPAE IF-UFRGS
Caixa Postal 15051, CEP 91501-970, Porto Alegre, RS, Brazil
magno-machado@uergs.edu.br, magnus@if.ufrgs.br*

Received (Day Month Year)

Revised (Day Month Year)

The high parton density regime of the Quantum Chromodynamics (QCD), where the physics of parton saturation is expected to be dominant, is briefly discussed. Some phenomenological aspects of saturation are described, mainly focusing on possible signatures of the non-linear QCD dynamics in the heavy quark production in electron-proton/nucleus collisions. Implications of these effects in the heavy quark production in ultraperipheral heavy-ion collisions are also presented.

Keywords: Quantum Chromodynamics; Heavy Quark Production; Parton Saturation.

PACS Nos.: 12.38.-t; 13.85.-t; 24.85.+p

1. Introduction

The understanding and analytic description of the QCD at high energies (small Bjorken x) has become an increasingly active subject of research, both from experimental and theoretical points of view (For a recent review, see e.g. ¹). These studies are mainly motivated by the violation of the unitarity (or Froissart-Martin bound ², which states that $\sigma_{tot} < C \ln^2(s)$ at asymptotically large energies s) by the solutions of the linear perturbative DGLAP ³ and BFKL ⁴ evolution equations. Since these evolution equations predict that the cross section rises obeying a power law on energy, new dynamical effects associated with the unitarity restoration are expected to stop its further growth ⁵. This expectation can be easily understood: while for large momentum transfer \mathbf{k}_\perp , the BFKL equation predicts that the mechanism $g \rightarrow gg$ populates the transverse space with a large number of small size gluons per unit of rapidity (the transverse size of a gluon with momentum \mathbf{k}_\perp is proportional to $1/\mathbf{k}_\perp$), for small \mathbf{k}_\perp the produced gluons overlap and fusion pro-

cesses, $gg \rightarrow g$, are equally important. Considering the latter process, the rise of the gluon distribution below a typical scale is slowed down, restoring the unitarity. That typical scale is energy dependent and is called saturation scale Q_{sat} . The saturation momentum sets the critical transverse size for the unitarization of the cross sections. In other words, unitarity is restored by including non-linear corrections in the evolution equations⁵. Such effects are small for $k_{\perp}^2 > Q_{\text{sat}}^2$ and very strong for $k_{\perp}^2 < Q_{\text{sat}}^2$, leading to the saturation of the scattering amplitude. The magnitude of Q_{sat} is associated to the behavior of the gluon distribution at high energies, and some estimates has been obtained. In general, the predictions are $Q_{\text{sat}} \sim 1$ GeV at HERA/RHIC and $Q_{\text{sat}} \sim 2 - 3$ GeV at LHC^{6,7}. In particular, it has been observed that the ep deep inelastic scattering (DIS) data at low x can be successfully described with the help of the saturation model⁶, which incorporates the main characteristics of the high density QCD approaches^{8,9,10}.

On the other hand, deep inelastic scattering on nuclei gives us a new possibility to reach high-density QCD phase without requiring extremely low values of x . The nucleus in this process serves as an amplifier for nonlinear phenomena. In order to understand this expectation and estimate the kinematic region where the high densities effects should be present, we can analyze the behavior of the function $\kappa(x, Q^2) \equiv \frac{3\pi^2\alpha_s}{2Q^2} \frac{xg_A(x, Q^2)}{\pi R_A^2}$, where xg_A is the gluon distribution on the target A of transverse size $R_A \propto A^{1/3}$ probed by a virtual probe of virtuality Q^2 . Such a function represents the probability of gluon-gluon interaction inside the parton cascade, and also is denoted the packing factor of partons in a parton cascade⁵. Considering that the condition $\kappa = 1$ specifies the critical line, which separates between the linear (low parton density) regime $\kappa \ll 1$ and the high density regime $\kappa \gg 1$, we can define the saturation momentum scale Q_{sat} given by $Q_{\text{sat}}^2(x; A) = \frac{3\pi^2\alpha_s}{2} \frac{xg_A(x, Q_{\text{sat}}^2(x; A))}{\pi R_A^2}$, below which the gluon density reaches its maximum value (saturates). At any value of x there is a value of $Q^2 = Q_{\text{sat}}^2(x)$ in which the gluonic density reaches a sufficiently high value that the number of partons stops to rise. This scale depends on the energy of the process [$xg \propto x^{-\lambda}$ ($\lambda \approx 0.3$)] and on the atomic number of the colliding nuclei [$R_A \propto A^{\frac{1}{3}} \rightarrow Q_s^2 \propto A^{\frac{1}{3}}$], with the saturation scale for nuclear targets larger than for nucleon ones. This result motivates more extensive studies of nuclear collisions and, in particular, of electron-nucleus collisions at high energies, where nuclear medium effects are reduced in comparison with AA collisions.

In what follows we present a brief review of some signatures of the high parton density regime, with special emphasis on the heavy quark production in the saturation scenario. In the next section, we present a brief review of the saturation approaches for deep inelastic scattering process. In section 3 we discuss the property of geometric scaling in the inclusive charm production. Moreover, in Section 4, we consider the heavy quark production in photonuclear process. In Section 5 the possibility of using ultraperipheral heavy ion collisions as a photonuclear collider is analyzed and some predictions for the saturation effects in the heavy quark

production are presented. Finally, in Section 6 we summarize our main conclusions.

2. Overview on the Saturation Approaches

We start from the space-time picture of the electron-proton/nuclei processes¹¹. The deep inelastic scattering $ep(A) \rightarrow e + X$ is characterized by a large electron energy loss ν (in the target rest frame) and an invariant momentum transfer $q^2 \equiv -Q^2$ between the incoming and outgoing electron such that $x = Q^2/2m_N\nu$ is fixed (m_N is the target mass). In terms of Fock states we then view the $ep(A)$ scattering as follows: the electron emits a photon ($|e \rightarrow |e\gamma \rangle$) with $E_\gamma = \nu$ and $p_{t\gamma}^2 \approx Q^2$, after the photon splits into a $q\bar{q}$ ($|e\gamma \rightarrow |eq\bar{q} \rangle$) and typically travels a distance $l_c \approx 1/m_N x$, referred as the coherence length, before interacting in the target. For small x , the photon converts to a quark pair at a large distance before its scattering. Consequently, the space-time picture of the DIS in the target rest frame can be viewed as the decay of the virtual photon at high energy into a quark-antiquark pair (color dipole), which subsequently interacts with the target. In the small x region, the color dipole crosses the target with fixed transverse distance \mathbf{r}_\perp between the quarks. The interaction $\gamma^*p(A)$ is further factorized and is given by¹¹,

$$\sigma_{L,T}^{*\gamma^*p(A)}(x, Q^2) = \sum_f \int dz d^2\mathbf{r}_\perp |\Psi_{L,T}^{(f)}(z, \mathbf{r}_\perp, Q^2)|^2 \sigma_{dip}^{p(A)}(x, \mathbf{r}_\perp), \quad (1)$$

where z is the longitudinal momentum fraction of the quark of flavor f . The photon wave functions $\Psi_{L,T}$ are determined from light cone perturbation theory (For a review see, e. g., Ref. ¹²).

The dipole hadron (nucleus) cross section σ_{dip} contains all information about the target and the strong interaction physics. Currently, the most complete QCD based effective theory that describes the physics of hadronic interactions at very high energies is the Color Glass Condensate (CGC)¹⁰. This represents the small x gluonic components in a hadronic wavefunction and is named so since: *Color* stands for the charge carried by the gluons; *Glass* stands for a clear separation of time scales between the fast and slow degrees of the wavefunction; *Condensate* stands for the high density of gluons which can reach values of order $\mathcal{O}(1/\alpha_s)$. The regime of a CGC is characterized by the limitation on the maximum phase-space parton density that can be reached in the hadron/nuclear wavefunction (parton saturation) and very high values of the QCD field strength $F_{\mu\nu} \approx 1/\alpha_s$. The large values of the gluon distribution at saturation suggest the use of semi-classical methods, which allow to describe the small- x gluons inside a fast moving nucleus by a classical color field¹³. In the CGC formalism¹⁰, σ_{dip} can be computed in the eikonal approximation, resulting

$$\sigma_{dip}(x, r_\perp) = 2 \int d^2\mathbf{b}_\perp [1 - S(x, \mathbf{r}_\perp, \mathbf{b}_\perp)] , \quad (2)$$

where S is the S-matrix element at fixed impact parameter \mathbf{b}_\perp which encodes all the information about the hadronic scattering, and thus about the non-linear and quan-

tum effects in the hadron wave function. It can be obtained by solving the functional evolution equation in the rapidity $y \equiv \ln(1/x)$ derived by Jalilian-Marian, Iancu, McLerran, Weigert, Leonidov and Kovner (JIMWLK) ¹⁰. An equivalent equation was developed by Balitsky ⁸. These equations form a set of coupled equations, and as such are very difficult to deal with analytically. An approximated equation which allows to deal with scattering at or near the unitarity limit was suggested by Kovchegov ⁹, and can be considered a mean field approximation for the Balitsky-JIMWLK equations. While the Kovchegov equation is not so complete it does have the advantage of being a precise nonlinear equation for a function. Many interesting limits of the Kovchegov equation has been understood by analytical methods, with the main properties for the S-matrix being: (a) for the interaction of a small dipole ($\mathbf{r}_\perp \ll 1/Q_{\text{sat}}$), $S(\mathbf{r}_\perp) \approx 1$, which characterizes that this system is weakly interacting; (b) for a large dipole ($\mathbf{r}_\perp \gg 1/Q_{\text{sat}}$), the system is strongly absorbed which implies $S(\mathbf{r}_\perp) \ll 1$. This property is associate to the large density of saturated gluons in the hadron wave function.

In our analysis we will consider the phenomenological saturation model proposed in Ref. ⁶ which encodes the main properties of the non-linear QCD approaches. In this model one has,

$$\frac{\sigma_{dip}(x, \mathbf{r}_\perp)}{\sigma_0} = 1 - S(x, \mathbf{r}_\perp); \quad S = \exp \left[-\frac{Q_{\text{sat}}^2(x) \mathbf{r}_\perp^2}{4} \right], \quad (3)$$

with σ_{dip}/σ_0 the scattering amplitude, averaged over all impact parameters \mathbf{b}_\perp , and $Q_{\text{sat}}^2 \simeq \Lambda^2 e^{\lambda \ln(x_0/x)}$. The parameters of the model were constrained from the HERA small x data, coming out typical values of order 1-2 GeV² for the momentum scale. We have that when $Q_{\text{sat}}^2(x) \mathbf{r}_\perp^2 \ll 1$, the model reduces to color transparency, whereas as one approaches the region $Q_{\text{sat}}^2(x) \mathbf{r}_\perp^2 \approx 1$, the exponential takes care of resumming many gluon exchanges, in a Glauber-inspired way. Intuitively, this is what happens when the proton starts to look dark. Moreover, a smooth transition to the photoproduction limit is obtained with a modification of the Bjorken variable as $x \rightarrow \tilde{x} = (Q^2 + 4m_f^2)/W_{\gamma p}^2$ and the large x threshold corrections are accounted for by multiplying equation above by a factor $(1-x)^n$ [$n = 5(7)$ for light (heavy) quarks].

One of the shortcomings of the saturation model is that the impact parameters are averaged over. Thus there may be saturation at the center of the proton, but the averaging gives much weight to the edges of the proton, where saturation is not present. The implicit assumption in the approach is that the proton is treated as being homogeneous in the transverse plane. In such case, the impact parameter profile is given by the Heaviside function, $s(\mathbf{b}_\perp) = \Theta(b_0 - b_\perp)$, and is considered to be peaked at central impact parameter, namely at $\mathbf{b}_\perp = 0$. Actually, this procedure is oversimplified and more realistic profiles can be considered. For phenomenological purposes a Gaussian or a hard sphere assumption are commonly taken into account. Recently, the impact parameter dipole saturation model ¹⁴ was developed, recovering the known Glauber-Mueller dipole cross section as well as the DGLAP evolution

has been included in the dipole cross section¹⁵. Using a simple parameterization for the S-matrix element in terms of the gluon distribution, those authors have obtained a smooth matching onto the DGLAP evolution, at least in the leading order DGLAP formalism, improving significantly the fit to the data in the large Q^2 region.

Therefore, despite the saturation model to be very successful in describing HERA data, its functional form is only an approximation of the theoretical non-linear QCD approaches. Recently, a lot of work has been done to found analytical solutions from the saturation formalisms. Along these lines, currently intense theoretical studies has been performed towards an understanding of the BFKL approach in the border of the saturation region¹⁶. In particular, a parameterization for the dipole cross section has been implemented in Ref.¹⁷, where this quantity was constructed to smoothly interpolate between the limiting behaviors analytically under control: the solution of the BFKL equation for small dipole sizes, $\mathbf{r}_\perp \ll 1/Q_{\text{sat}}(x)$, and the Levin-Tuchin law¹⁸ for larger ones, $\mathbf{r}_\perp \gg 1/Q_{\text{sat}}(x)$. The model has been used in phenomenological studies on vector meson production¹⁹, diffractive processes²⁰ and longitudinal structure function F_L ²¹ at HERA, as well as neutrino-nucleon total cross section²².

3. Heavy quarks in lepton-hadron collisions - Geometric Scaling

An important feature of the available saturation approaches is the prediction of the geometric scaling. Namely, the total γ^*p cross section at large energies is not a function of the two independent variables x and Q^2 , but is rather a function of the single variable $\tau = Q^2/Q_{\text{sat}}^2$. In Ref.¹⁶ the authors have demonstrated that the geometric scaling predicted at low momenta $Q^2 \leq Q_{\text{sat}}^2(x)$ is preserved by the BFKL evolution up to relatively large virtualities, within the kinematical window $Q_{\text{sat}}^2 \leq Q^2 \ll Q_{\text{sat}}^4/\Lambda_{\text{QCD}}^2$. As demonstrated in Ref.²³, the HERA data on the proton structure function F_2 are consistent with scaling at $x \leq 0.01$ and $Q^2 \leq 400 \text{ GeV}^2$. Similar behavior have been observed in exclusive processes²⁴ and in the nuclear case²⁵.

In this section we analyze the geometric scaling in the inclusive charm production²⁶. From the experimental point of view, the HERA experiments have published data for the contribution of charmed meson production to the structure function F_2 . This allows one to single out the charm contribution F_2^c to the total structure function and thus to investigate if the property of geometric scaling is also present in this observable. Before presenting our results, lets perform a qualitative analysis of the inclusive charm production using the saturation model⁶ in order to shed light on the dipole configurations dominating the process in the relevant kinematical limits and show how the geometric scaling comes out. A characteristic feature in heavy quark production within the color dipole approach is that the process is dominated by small size dipole configurations²⁷. The overlap function weighting the dipole cross section is peaked at $\mathbf{r}_\perp \sim 1/m_c \simeq 0.1 \text{ fm}$ even for sufficiently low

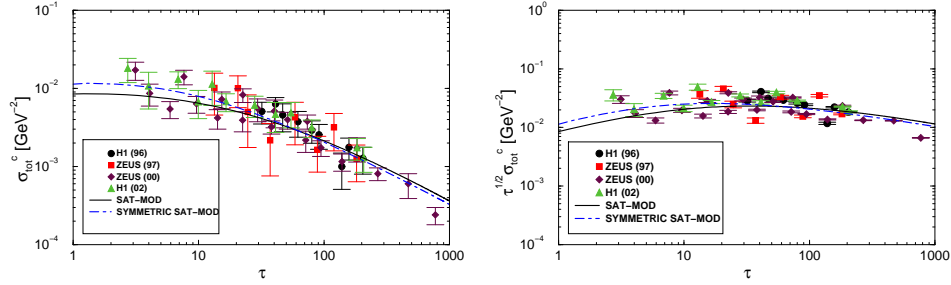


Fig. 1. Experimental data on inclusive charm production plotted versus the scaling variable. The curves are the saturation model (solid line) and symmetric saturation model (dashed lines).

Q^2 values. As a consequence, charm production is dominated by color transparency and saturation effects are not important there, i.e. $\sigma_{dip} \simeq \sigma_0 Q_{\text{sat}}^2(x) r_\perp^2/4$.

For the HERA kinematical region, we have $Q_{\text{sat}}^2 \approx 1 \text{ GeV}^2$, which implies that the relation $Q_{\text{sat}}^2 < Q^2 + \mu_c^2$ is ever satisfied, where $\mu_c^2 \equiv 4m_c^2$. Consequently, we can define two kinematical regimes depending of the relation between Q^2 and μ_c^2 . For $Q^2 \gg \mu_c^2$ we have scaling with logarithmic enhancement coming from aligned jet configurations, whereas for $Q^2 \ll \mu_c^2$ only symmetric dipole configurations contribute. Therefore, one obtains that the total cross section reads as,

$$\sigma_{tot}^{c\bar{c}} \sim \frac{\sigma_0 Q_{\text{sat}}^2(x)}{Q^2} \left(1 + \ln \frac{Q^2}{\mu_c^2} \right) \Theta(Q^2 - \mu_c^2) + \frac{\sigma_0 Q_{\text{sat}}^2(x)}{\mu_c^2} \Theta(\mu_c^2 - Q^2), \quad (4)$$

where the first term provides the behavior $1/\tau$ at large τ whereas the second term leads to a smooth transition down to the asymptotic (τ -independent) behavior at small τ .

An analytical expression for the τ dependence of the inclusive charm production can also be obtained in a less model dependent way. For this purpose we will make use of the symmetric saturation model²⁸, where the energy evolution of the proton leads to the parton multiplication and the transverse momentum scale $Q_{\text{sat}}(x)$ appears. The main assumption is that the evolved proton can be described by a collection of independent dipoles at the time of the interaction whose sizes are distributed around $1/Q_{\text{sat}}$. The rate of growth of the parton densities is assumed to be $Q_{\text{sat}}^2(x)/\Lambda^2$ and the symmetry between low and high virtualities in γp interactions comes from the symmetry in the dipole-dipole cross section. In the HERA kinematical regime, i.e. $Q_{\text{sat}}^2 < \mu_c^2$, the inclusive charm production is given by,

$$\sigma_{tot}^{c\bar{c}}(\tau) = \frac{N_{c\bar{c}}}{\Lambda^2 \nu_{>}} \left\{ 1 - \exp \left[-\frac{\nu_{>}}{\tau + \tau_c} (1 + \log(\tau + \tau_c)) \right] \right\}, \quad (5)$$

where $\tau_c = \mu_c^2/Q_{\text{sat}}^2(x)$ and the parameters N , Λ^2 and $\nu_{(>,<)}$ are taken from the data fit in Ref.²⁸. Here, we make the simplified assumption that the coupling with the dipole is flavor blind, in such way that $N_{c\bar{c}} = (2/5)N$, with N being the global normalization describing F_2 data. The factor $2/5$ corresponds to the charge fraction

$e_c^2/(\sum e_{u,d,s}^2 + e_c^2)$. Once the parameters are fitted to proton structure function data, our prediction for the τ dependence in the inclusive charm production is parameter free.

In Fig. 1 we show the experimental data on the total cross section for the inclusive charm production plotted versus scaling variable τ , with Q_{sat} from the saturation model. We see the data exhibit geometric scaling for the whole Q^2 range, verifying a transition in the behavior on τ of the cross section from a smooth dependence at small τ and an approximated $1/\tau$ behavior at large τ . The transition point is placed at $\mu_c^2 = 4m_c^2$, which takes values of order 10 GeV^2 for a charm mass $m_c = 1.5 \text{ GeV}$. This turns out in $\tau \simeq 10$ since at HERA $Q_{\text{sat}}^2 \simeq 1 \text{ GeV}^2$. The asymptotic $1/\tau$ dependence reflects the fact the charm production cross section scales as Q_{sat}^2/Q^2 modulo a logarithmic correction $\sim \ln(Q^2/\mu_c^2)$, with energy dependence driven by the saturation scale. The mild dependence at $\tau \leq \mu_c^2$ corresponds to the fact the cross section scales as Q_{sat}^2/μ_c^2 towards the photoproduction limit, but with the same energy behavior given by the saturation scale. In Fig. 1, we also found a symmetry between the regions of large and small τ for the function $\sqrt{\tau} \sigma_{\text{tot}}^{c\bar{c}}$ with respect the transformation $\tau \leftrightarrow 1/\tau$ in the whole region of τ . The features present in the inclusive charm production data can be well reproduced in the phenomenological saturation model, corresponding to the solid curve in Fig. 1. The symmetric saturation model also provides similar results, as shown in the dot-dashed lines. Disregarding the Glauber-like resummation in this model, the expression gets simplified to $\sigma_{\text{tot}}^{c\bar{c}} \propto \frac{1}{\tau + \tau_c} [1 + \log(\tau + \tau_c)]$, and the symmetric pattern is easily verified.

In the HERA kinematic domain the saturation momentum $Q_{\text{sat}}^2(x)$ stays below the hard scale $\mu_c^2 = 4m_c^2$, implying that charm production probes mostly the color transparency regime and saturation corrections are not very important. However, as the saturation scale rises with the energy and the atomic number, we expect that at larger energies and nuclear collisions a new kinematic regime where $Q_{\text{sat}}^2(x) \geq \mu_c^2$ will be probed. Recently, the production of open charm in heavy ion collisions in the CGC framework has been considered in Ref. ²⁹. The main prediction is the approximate scaling of the cross section with the number of participants (N_{part}) in the forward rapidity region, where the saturation scale exceeds the charm quark mass. This result is in contrast with usual expectation for a hard process of scaling with the number of collisions (N_{coll}). These results provide a strong motivation for further investigations (See, e.g. Refs. ^{30,31,32}).

4. Heavy quark production in photonuclear process

In this section, we report our investigations on the high energy heavy quark photoproduction on nuclei targets using the saturation hypothesis ²⁷. In particular, we study them considering the approach proposed in Ref. ³³, which extends the saturation model for scattering on nuclei and gives a reasonable parameter-free description of the experimental data on nuclear structure function. In this model the

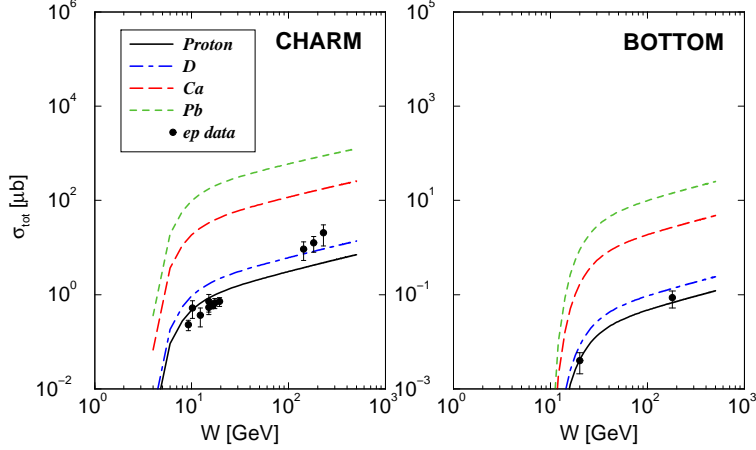


Fig. 2. The total nuclear cross section for charm and bottom photoproduction as a function of energy $W_{\gamma A}$ for distinct nuclei.

dipole-nucleus cross section is given by ³³,

$$\sigma_{dip}^{\text{nucleus}}(x, \mathbf{r}_{\perp}^2, A) = 2 \int d^2 \mathbf{b}_{\perp} \left\{ 1 - \exp \left[-\frac{1}{2} A T_A(\mathbf{b}_{\perp}) \sigma_{dip}^{\text{nucleon}}(x, \mathbf{r}_{\perp}^2) \right] \right\}, \quad (6)$$

where \mathbf{b}_{\perp} is the impact parameter of the center of the dipole relative to the center of the nucleus and the integrand gives the total dipole-nucleus cross section for a fixed impact parameter. The nuclear profile function is labeled by $T_A(\mathbf{b}_{\perp})$. The above equation sums up all the multiple elastic rescattering diagrams of the $q\bar{q}$ pair and is justified for large coherence length, where the transverse separation \mathbf{r}_{\perp} of partons in the multiparton Fock state of the photon becomes as good a conserved quantity as the angular momentum, *i. e.* the size of the pair \mathbf{r}_{\perp} becomes eigenvalue of the scattering matrix. Here, the dipole cross section for the nucleon target (proton), $\sigma_{dip}^{\text{nucleon}}(x, \mathbf{r}_{\perp}^2)$, is given by the saturation model [Eq. (3)]. The photoproduction cross section reads as,

$$\sigma_{tot}(\gamma A \rightarrow Q\bar{Q}X) = \int dz d^2 \mathbf{r}_{\perp} |\Psi_T^{Q\bar{Q}}(z, \mathbf{r}_{\perp}, Q^2 = 0)|^2 \sigma_{dip}^{\text{nucleus}}(x, \mathbf{r}_{\perp}), \quad (7)$$

where the dipole-nucleus cross section is given by Eq. (6) and only the transverse wavefunction for the heavy quark-antiquark pair $Q\bar{Q}$ contributes at $Q^2 \rightarrow 0$.

In Fig. 2 are shown the results for the charm and bottom photoproduction cross section as a function of energy for different nuclei, including the proton case. The results present mild growth on $W_{\gamma A}$ at high energies stemming from the saturation model, whereas the low energy region is consistently described through the large- x threshold factor ²⁷. For the proton, the experimental data from HERA and fixed target collisions are also included for comparison. The result for charm underestimates data by a factor 2 at $W_{\gamma p} \simeq 200$ GeV, whereas is consistent with the measurements of bottom cross section. Concerning charm production, the measured

cross sections present a well known steeper behavior on energy even at electroproduction, suggesting that further resummations in the original saturation model are needed in order to produce the larger growth on energy appearing in the charm measurements. We believe that the better result for bottom happens to be a mismatch between a large uncertainty in the experimental measurement and the lower bottom mass $m_b = 4.5$ GeV considered here. For the nuclear case, we predict that their absolute values are rather large, reaching $\approx 2 \cdot 10^3$ and $\approx 40 \mu b$ for charm and bottom for lead at $W_{\gamma A} = 10^3$ GeV.

The simple intuitive dipole approach considered above has a deep connection with a more general theoretical formalism. Namely, it is equivalent, at leading logarithmic approximation, to the high energy k_\perp -factorization (semihard) approach³⁴. In this framework, the relevant QCD diagrams are considered with the virtualities and polarizations of the initial partons, carrying information on their transverse momenta. The scattering processes are described through the convolution of off-shell matrix elements with the unintegrated parton distribution, $\mathcal{F}(x, \mathbf{k}_\perp)$. The characteristic feature is the LO cross section in this approach resumming most of the NLO and even NNLO diagrams contributing to the process in the collinear formalism. As heavy quark photoproduction is concerned, considering only the direct component of the photon, the cross section reads as³⁴,

$$\sigma_{tot}(\gamma A \rightarrow Q\bar{Q}X) = \frac{\alpha_{em} e_Q^2}{\pi} \int dz d^2\mathbf{p}_{1\perp} d^2\mathbf{k}_\perp \frac{\alpha_s(\mu^2) \mathcal{F}(x, \mathbf{k}_\perp^2)}{\mathbf{k}_\perp^2} \times \left\{ [z^2 + (1-z)^2] \left(\frac{\mathbf{p}_{1\perp}}{D_1} + \frac{(\mathbf{k}_\perp - \mathbf{p}_{1\perp})}{D_2} \right)^2 + m_Q^2 \left(\frac{1}{D_1} + \frac{1}{D_2} \right)^2 \right\},$$

where $D_1 \equiv \mathbf{p}_{1\perp}^2 + m_Q^2$ and $D_2 \equiv (\mathbf{k}_\perp - \mathbf{p}_{1\perp})^2 + m_Q^2$. The transverse momenta of the heavy quark (antiquark) are denoted by $\mathbf{p}_{1\perp}$ and $\mathbf{p}_{2\perp} = (\mathbf{k}_\perp - \mathbf{p}_{1\perp})$, respectively. The heavy quark longitudinal momentum fraction is labeled by z . For the scale μ in the strong coupling constant we use the prescription $\mu^2 = \mathbf{k}_\perp^2 + m_Q^2$. The unintegrated gluon distribution $\mathcal{F}(x, \mathbf{k}_\perp^2)$ is directly related to the Fourier transform of the dipole-nucleon (nucleus) total cross section, as follows

$$\frac{\mathcal{F}(x, \mathbf{k}_\perp^2)}{\mathbf{k}_\perp^2} = \frac{3}{4\pi\alpha_s} \int d^2\mathbf{b}_\perp \int \frac{d^2\mathbf{r}_\perp}{(2\pi)^2} e^{i\mathbf{k}_\perp \cdot \mathbf{r}_\perp} [\sigma_{dip}(x, \mathbf{r}_\perp \rightarrow \infty, \mathbf{b}_\perp) - \sigma_{dip}(x, \mathbf{r}_\perp, \mathbf{b}_\perp)].$$

For the saturation model this quantity takes a simple analytical form, which reads for the proton and nucleus case as³⁵,

$$\mathcal{F}_{\text{proton}}^{\text{sat}}(x, \mathbf{k}_\perp) = \frac{3\sigma_0}{4\pi^2\alpha_s} \left(\frac{\mathbf{k}_\perp^2}{Q_{\text{sat}}^2(x)} \right) \exp \left(-\frac{\mathbf{k}_\perp^2}{Q_{\text{sat}}^2(x)} \right), \quad (8)$$

$$\mathcal{F}_{\text{nucleus}}^{\text{sat}}(x, \mathbf{k}_\perp, \mathbf{b}_\perp) = \frac{3}{2\pi^2\alpha_s} \left(\frac{\mathbf{k}_\perp^2}{Q_{sA}^2(x, \mathbf{b}_\perp)} \right) \exp \left(-\frac{\mathbf{k}_\perp^2}{Q_{sA}^2(x, \mathbf{b}_\perp)} \right), \quad (9)$$

where the expression for nuclei is obtained under the assumption of dominance of color transparency (small dipole configurations) in the dipole cross section, which

is correct for the particular case of heavy quark production. The nuclear saturation scale is given by $Q_{sA}^2(x, b_\perp) = \frac{1}{2} A T_A(b_\perp) \sigma_0 Q_{\text{sat}}^2(x)$. We call attention to the scaling pattern on the variable $\tau = \mathbf{k}_\perp^2 / Q_{sA}^2$, which implies scaling on τ also in the nuclear heavy quark production. In our further analysis, they will be compared with the simple ansatz $\mathcal{F}_{\text{nuc}} = \frac{\partial x G_A(x, \mathbf{k}_\perp^2)}{\partial \ln \mathbf{k}_\perp^2}$, with $x G_A(x, Q^2)$ being the nuclear gluon distribution (see ^{27,35} for details in the numerical calculations).

On the other hand, in the collinear approach the cross section is given by a convolution between the partonic cross section for the subprocess $\gamma g \rightarrow Q\bar{Q}$ and the integrated gluon distribution for the nucleus $x G_A(x, Q^2)$. In our studies in Ref. ³⁵, one considers the EKS ³⁶ and AG ³⁷ parameterizations for this distribution. The EKS parameterization was obtained from a global fit of the nuclear experimental data using the DGLAP evolution equations, which is a linear evolution equation which does not consider dynamical saturation (high density) effects. In Ref. ³⁷ a procedure to include these effects in the nuclear gluon distribution was proposed, resulting in a parameterization for this distribution (AG parameterization), which also includes those present in the EKS parameterization. The AG parameterization predicts a stronger reduction of the growth of the gluon distribution at small values of x than the EKS one.

When the nuclear photoproduction cross section of heavy quarks is computed considering these different approaches, we have obtained that the k_\perp -factorization using EKS unintegrated gluon pdf (semihard approach) gives similar results to the collinear approach where nuclear effects (EKS parameterization) and high density corrections (AG parameterization) are taken into account. In particular, we have that the predictions using the AG parameterization in the collinear approach are similar to the semihard one, which does not consider high density effects. This demonstrate that in this process we cannot distinguish if the modification in the behavior of the cross section is associated to high density effects in the collinear approach or a generalization of the factorization without high density effects in the unintegrated gluon distribution. On the other hand, if these effects are present and the factorization of the cross section is given by the k_\perp -factorization, as is the case for the predictions from the saturation model, we have that the difference between the cross sections is large, which should allow to discriminate between the theoretical approaches. Therefore, the nuclear cross section would provide a strong test concerning the robustness of the saturation approach in describing the observables. The situation is less clear comparing the semihard approach and the collinear one. One possible interpretation for this result is that the expected enhancement in the semihard approach, associated to the resummation of the $(\alpha_s \ln \frac{\sqrt{s}}{m_Q})^n$ in the coefficient function, is not sizeable for inclusive quantities in the kinematic region of the future colliders. Probably, a more promising quantity to clarify this issue would be the transverse momentum \mathbf{p}_\perp distribution. In this case, the semihard approach seems to be in better agreement with experimental data in the pp collisions than the collinear approach ³⁴.

5. Heavy Quarks in Ultraperipheral Heavy Ion Collisions

The studies of saturation effects in nuclear processes shown that future electron-nucleus colliders at HERA and RHIC, probably could determine whether parton distributions saturate and constrain the behavior of the nuclear gluon distribution in the full kinematical range. However, until these colliders become reality we need to consider alternative searches in the current and/or scheduled accelerators which allow us to constrain the QCD dynamics. Recently, we have analyzed the possibility of using ultraperipheral heavy ion collisions (UPC's) as a photonuclear collider. In particular, we have studied the heavy quark production³⁹ assuming distinct approaches for the QCD evolution.

In heavy ion collisions the large number of photons coming from one of the colliding nuclei will allow to study photoproduction, with energies $W_{\gamma A}$ reaching to almost 1 TeV for the LHC. The photonuclear cross sections are given by the convolution between the photon flux from one of the nuclei and the cross section for the scattering photon-nuclei, with the photon flux $\frac{dN(\omega)}{d\omega}$ given by the Weizsacker-Williams method³⁸. The final expression for the production of heavy quarks in ultraperipheral heavy ion collisions is given by,

$$\sigma_{AA \rightarrow Q\bar{Q}X}(\sqrt{S_{NN}}) = \int_{\omega_{min}}^{\infty} d\omega \frac{dN(\omega)}{d\omega} \sigma_{\gamma A \rightarrow Q\bar{Q}X}(W_{\gamma A}^2 = 2\omega\sqrt{S_{NN}}) \quad (10)$$

where ω is the c.m.s. photon energy, $\omega_{min} = M_{Q\bar{Q}}^2/4\gamma_L m_p$ and $\sqrt{S_{NN}}$ is the c.m.s. energy of the nucleus-nucleus system. The Lorentz factor for LHC is $\gamma_L = 2930$, giving the maximum c.m.s. γN energy $W_{\gamma A} \approx 950$ GeV. The requirement that photoproduction is not accompanied by hadronic interaction (ultraperipheral collision) can be done by restricting the impact parameter b to be larger than twice the nuclear radius, $R_A = 1.2 A^{1/3}$ fm. An analytic approximation for AA collisions can be obtained using as integration limit $b > 2R_A$, producing

$$\frac{dN(\omega)}{d\omega} = \frac{2Z^2\alpha_{em}}{\pi\omega} \left[\bar{\eta} K_0(\bar{\eta}) K_1(\bar{\eta}) + \frac{\bar{\eta}^2}{2} (K_1^2(\bar{\eta}) - K_0^2(\bar{\eta})) \right], \quad (11)$$

where $\bar{\eta} = 2\omega R_A/\gamma_L$ and $K_{0,1}(x)$ are the modified Bessel functions. The typical values of x which will be probed in ultraperipheral heavy ion collisions, are given by $x = (M_{Q\bar{Q}}/2p)e^{-y}$, where $M_{Q\bar{Q}}$ is the invariant mass of the photon-gluon system and y the center of momentum rapidity. For Pb + Pb collisions at LHC energies the nucleon momentum is equal to $p = 2750$ GeV; hence $x = (M_{Q\bar{Q}}/5500 \text{ GeV})e^{-y}$. Therefore, the region of small mass and large rapidities probes directly the high energy (small x) behavior of the QCD dynamics present in the γA cross section. This demonstrates that ultraperipheral heavy ion collisions at LHC represents a very good tool to constrain the high energy regime of the QCD dynamics.

In what follows we summarize our analysis on photonuclear production of heavy quarks at UPC's³⁹. In order to do this, one considers the available high energy approaches. Namely, the usual collinear approach, the semihard formalism and the

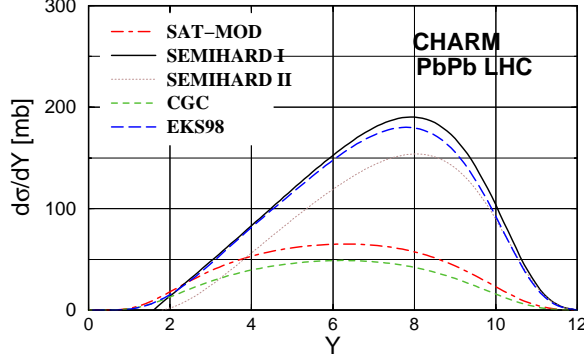


Fig. 3. Rapidity distribution for charm production in ultraperipheral heavy ion collisions.

phenomenological saturation reviewed in the previous section. As an additional analysis, we also consider the Color Glass Condensate (CGC) formalism. This puts into perspective the most recent representative high energy approaches and allow us to find out the observables and/or distributions which could disentangle them at the planned colliders.

In Refs. ⁴⁰ the heavy quark production in UPC's has been analyzed in the CGC formalism. In Ref. ³⁹, we have improved that analysis using a realistic photon flux and a color field correlator including quantum radiation effects. The differential cross section on rapidity reads as ³⁹,

$$\frac{d\sigma_{AA \rightarrow Q\bar{Q}X}}{dY} = \omega \frac{dN(\omega)}{d\omega} \frac{\alpha_{em} e_Q^2}{2\pi} \int_0^{+\infty} d\mathbf{k}_\perp^2 R_A^2 \tilde{C}(\mathbf{k}_\perp) \left\{ 1 + \frac{4(\mathbf{k}_\perp^2 - m_Q^2)}{k_\perp \bar{\mu}_Q^2} \operatorname{arctanh} \frac{k_\perp}{\bar{\mu}_Q^2} \right\},$$

where we define the rapidity $Y \equiv \ln(1/x) = \ln(2\omega \gamma_L / 4m_Q^2)$. The quark charge is labeled as e_Q and one uses the notation $\bar{\mu}_Q^2 \equiv \sqrt{\mathbf{k}_\perp^2 + 4m_Q^2}$. In Ref. ³⁹, we obtained the following analytical expression for the color field correlator, considering that it is directly related to the Fourier transform of the dipole-nucleus total cross section,

$$\tilde{C}(x, \mathbf{k}_\perp) = \left(\frac{4\pi}{Q_{sA}^2(x)} \right) \exp \left(-\frac{\mathbf{k}_\perp^2}{Q_{sA}^2(x)} \right), \quad (12)$$

where we have assumed $Q_{sA}^2(x) = A^{1/3} Q_{sat}^2(x)$. We believe that this input is more suitable for realistic computations because it includes quantum evolution in the formalism and reproduces most part of the phenomenological features of the saturation model for the nucleus case. It is worth mentioning the direct relation between the color field correlator and the unintegrated gluon distribution, given by $\mathcal{F}(x, \mathbf{k}_\perp) = (3R_A^2/8\pi^2\alpha_s) \mathbf{k}_\perp^2 C(x, \mathbf{k}_\perp)$.

In Fig. 3 is shown the charm rapidity distribution for the distinct high energy approaches considered. The collinear result is denoted by the long-dashed

curves, where we have employed the EKS98 parameterization for the collinear nuclear gluon function (See also Ref. ⁴¹). The solid and dotted lines label the semi-hard (k_{\perp} -factorization) results, where one has used the unintegrated gluon distribution $\mathcal{F}_{\text{nuc}}(x, k_{\perp}^2; A)$ discussed in the previous section. Two possibilities for the nucleon gluon distribution were considered: (I) GRV94(LO) - solid line - and (II) GRV98(LO) - dotted line. The saturation model results are denoted by the dot-dashed line. The CGC prediction is denoted by the dashed line. We have that the predictions for the collinear approach and the semihard formalism are similar and give somewhat larger values than the saturation and CGC results. One possible interpretation for the similarity between the predictions of the semihard approach and the collinear one is that the expected enhancement in the k_{\perp} -factorization formalism is not sizeable for inclusive quantities in the kinematic region of the future colliders ³⁴. Our phenomenological ansatz within the CGC formalism gives similar results as the saturation model, but should be noticed that the physical assumptions in those models are distinct. While the saturation model considers multiple scattering on single nucleons, our expression for the dipole-nucleus cross section in the CGC formalism assumes scattering on a black area filled by partons coming from many nucleons.

Let us present the numerical calculation of their total cross section at UPC's. We focus mostly on LHC domain where small values of x would be probed. The results are presented in Table 1. The collinear approach gives a larger rate, followed by the semihard approach. The saturation model and CGC formalisms give similar results, including a closer ratio for charm to bottom production. Concerning the CGC approach, our phenomenological educated guess for the color field correlator seems to produce quite reliable estimates. Therefore, the photonuclear production of heavy quarks allow us to constraint already in the current nuclear accelerators the QCD dynamics since the main features from photon-nuclei collisions hold in the UPC reactions. Our results shown that an experimental analysis of this process can be useful to constrain the QCD dynamics at high energies.

6. Summary

The perturbative QCD has furnished a remarkably successful framework to interpret a wide range of high energy lepton-lepton, lepton-hadron and hadron-hadron processes. Through global analysis of these processes, detailed information on the parton structure of hadrons, especially the nucleon, has been obtained. The existing global analysis have been performed using the standard DGLAP evolution equations. However, in the small x region the DGLAP evolution equations are expected to breakdown, since new dynamical effects associated to the high parton density must occur in this kinematical region.

Research in the field of QCD at high parton density deals both with fundamental theoretical issues, such as unitarity of strong interactions at high energies, and with the challenge of describing experimental data coming, at present, from HERA and

Table 1. *The photonuclear heavy quark total cross sections for UPC's at LHC.*

$Q\bar{Q}$	Collinear	SAT-MOD	SEMIHARD I (II)	CGC
$c\bar{c}$	2056 mb	862 mb	2079 (1679.3) mb	633 mb
$b\bar{b}$	20.1 mb	10.75 mb	18 (15.5) mb	8.9 mb

RHIC and expected exciting physics of forthcoming experiments at LHC. Over the past few years much theoretical effort has been devoted towards the understanding of the growth of the total scattering cross sections with energy. These studies are mainly motivated by the violation of the unitarity (or Froissart) bound by the solutions of the linear perturbative DGLAP and BFKL evolution equations. Since these evolution equations predict that the cross section rises obeying a power law of the energy, violating the Froissart bound, unitarity corrections are expected to stop its further growth.

In this paper we have presented a brief review of the basic concepts present in the high density approaches and discussed some aspects of the rapidly developing field of QCD at high parton density in ep , eA and AA collisions. The successful description of all inclusive and diffractive deep inelastic data at the collider HERA, as well as some recent results from RHIC, by saturation models suggests that these effects might become important in the energy regime probed by current colliders. In particular, the remarkable property of geometric scaling verified in the data indicate that the experiments are in a kinematical region which probe QCD in the non-linear regime of high parton density. These results show that the transition between the linear and non-linear regimes in eA processes at high energies will occur in a perturbative regime, justifying perturbative QCD approaches. Our recent studies shown that an alternative for eA colliders is the study of saturation effects in ultraperipheral heavy ion collisions.

Acknowledgments

This work was partially financed by the Brazilian funding agencies CNPq and FAPERGS.

1. E. Iancu and R. Venugopalan, arXiv:hep-ph/0303204.
2. M. Froissart, Phys. Rev. **123**, 1053 (1961); A. Martin, Phys. Rev. **129**, 1432 (1963).
3. V.N. Gribov and L.N. Lipatov, Sov. J. Nucl. Phys. **15**, 438 (1972); G. Altarelli and G. Parisi, Nucl. Phys. **B126**, 298 (1977); Yu.L. Dokshitzer, Sov. Phys. JETP **46**, 641 (1977).
4. L. N. Lipatov, Sov. J. Nucl. Phys. **23**, 338 (1976); E. A. Kuraev, L. N. Lipatov, V. S. Fadin, JETP **45**, 1999 (1977); I. I. Balitsky, L. N. Lipatov, Sov. J. Nucl. Phys. **28**, 822 (1978).
5. L. V. Gribov, E. M. Levin and M. G. Ryskin, Phys. Rept. **100**, 1 (1983).
6. K. Golec-Biernat and M. Wüsthoff, Phys. Rev. D **59**, 014017 (1999), *ibid.* **D60** 114023 (1999).

7. V. P. Gonçalves, Phys. Lett. B **495**, 303 (2000); M. B. Gay Ducati and V. P. Gonçalves, Phys. Lett. B **466**, 375 (1999).
8. I. I. Balitsky, Nucl. Phys. B **463**, 99 (1996).
9. Yu. Kovchegov, Phys. Rev. D **60**, 034008 (1999).
10. E. Iancu, A. Leonidov, L. McLerran, Nucl. Phys. A **692**, 583 (2001); E. Ferreiro, E. Iancu, A. Leonidov, L. McLerran, Nucl. Phys. A **703**, 489 (2002); J. Jalilian-Marian, A. Kovner, L. McLerran and H. Weigert, Phys. Rev. D **55**, 5414 (1997); J. Jalilian-Marian, A. Kovner and H. Weigert, Phys. Rev. D **59**, 014014 (1999), *ibid.* **59**, 014015 (1999), *ibid.* **59** 034007 (1999); A. Kovner, J. Guilherme Milhano and H. Weigert, Phys. Rev. D **62**, 114005 (2000); H. Weigert, Nucl. Phys. A **703**, 823 (2002).
11. N. N. Nikolaev and B. G. Zakharov, Z. Phys. **C49**, 607 (1991); Z. Phys. **C53**, 331 (1992).
12. V. Barone and E. Predazzi, *High-Energy Particle Diffraction*, Springer-Verlag, Berlin Heidelberg, (2002).
13. L. D. McLerran and R. Venugopalan, Phys. Rev. D **49**, 2233 (1994); Phys. Rev. D **49**, 3352 (1994); Phys. Rev. D **50**, 2225 (1994).
14. H. Kowalski and D. Teaney, Phys. Rev. D **68**, 114005 (2003).
15. J. Bartels, K. Golec-Biernat and H. Kowalski, Phys. Rev. D **66**, 014001 (2002).
16. E. Iancu, K. Itakura and L. McLerran, Nucl. Phys. A **708**, 327 (2002).
17. E. Iancu, K. Itakura and S. Munier, Phys. Lett. B **590**, 199 (2004).
18. E. Levin and K. Tuchin, Nucl. Phys. B **573**, 833 (2000).
19. J. R. Forshaw, R. Sandapen and G. Shaw, Phys. Rev. D **69**, 094013 (2004).
20. J. R. Forshaw, R. Sandapen and G. Shaw, Phys. Lett. B **594**, 283 (2004).
21. V. P. Gonçalves and M. V. T. Machado, Eur. Phys. J. C (in press), arXiv:hep-ph/0406230.
22. M. V. T. Machado, Phys. Rev. D **70**, 053008 (2004).
23. A. M. Staśto, K. Golec-Biernat and J. Kwieciński, Phys. Rev. Lett. **86**, 596 (2001).
24. S. Munier and S. Wallon, Eur. Phys. J. C **30**, 359 (2003).
25. A. Freund, K. Rummukainen, H. Weigert and A. Schafer, Phys. Rev. Lett. **90**, 222002 (2003).
26. V. P. Gonçalves and M. V. T. Machado, Phys. Rev. Lett. **91**, 202002 (2003).
27. V. P. Gonçalves and M. V. T. Machado, Eur. Phys. J. C **30**, 387 (2003).
28. S. Munier, Phys. Rev. D **66**, 114012 (2002).
29. D. Kharzeev and K. Tuchin, Nucl. Phys. A **735**, 248 (2004).
30. F. Gelis and R. Venugopalan, Phys. Rev. D **69**, 014019 (2004).
31. K. Tuchin, arXiv:hep-ph/0401022.
32. J. P. Blaizot, F. Gelis and R. Venugopalan, Nucl. Phys. A **743**, 57 (2004).
33. N. Armesto, Eur. Phys. J. C **26**, 35 (2002).
34. B. Andersson *et al.* [Small x Collaboration], Eur. Phys. J. C **25**, 77 (2002); J. R. Andersen *et al.* [Small x Collaboration], Eur. Phys. J. C **35**, 67 (2004).
35. V. P. Gonçalves and M. V. T. Machado, Eur. Phys. J. C **32**, 501 (2004).
36. K. J. Eskola, V. J. Kolhinen and C. A. Salgado, Eur. Phys. J. C **9**, 61 (1999).
37. A. L. Ayala Filho and V. P. Gonçalves, Eur. Phys. J. C **20**, 343 (2001).
38. C. A. Bertulani and G. Baur, Phys. Rept. **163**, 299 (1988); G. Baur, K. Hencken, D. Trautmann, S. Sadovsky and Y. Kharlov, Phys. Rept. **364**, 359 (2002).
39. V. P. Gonçalves and M. V. T. Machado, Eur. Phys. J. C **31**, 371 (2003).
40. F. Gelis and A. Peshier, Nucl. Phys. A **697**, 879 (2002); Nucl. Phys. A **707**, 175 (2002).
41. V. P. Gonçalves and C. A. Bertulani, Phys. Rev. C **65**, 054905 (2002).